J. Ocean Univ. China (Oceanic and Coastal Sea Research)
https://doi.org/10.1007/s11802-022-4711-1
ISSN 1672-5182, 2022 21 (1): 81-90
http://www.ouc.edu.cn/xbywb/
E-mail:xbywb@ouc.edu.cn

Retrieval of Significant Wave Height Under Typhoon Conditions from Gaofen-3 SAR Imagery

WANG Xiaochen[1), 2)], HAN Bing[1), 2), *], ZHONG Lihua[1), 2)], and YUAN Xinzhe[3)]

1) *Aerospace Information Research Institute*, *Chinese Academy of Science*, *Beijing* 100190, *China*
2) *Key Laboratory of Technology in Geo-Spatial Information Processing and Application Systems*, *Aerospace Information Research Institute*, *Chinese Academy of Science*, *Beijing* 100190, *China*
3) *The National Satellite Ocean Applications Center*, *Beijing* 100081, *China*

(Received September 2, 2020; revised November 9, 2020; accepted December 11, 2020)

Abstract The objective of this paper is to propose an empirical method to inverse significant wave height (SWH) under typhoon conditions from collected dual-polarization Gaofen (GF)-3 synthetic aperture radar (SAR) imagery. The typhoon scenes were captured from narrow scan (NSC) and wide scan (WSC) images, and collocated with European Center for Medium-Range Weather Forecasts reanalysis data of (ECMWF). To improve the quality of GF-3 SAR images, the recalibration over rainforest and de-scalloping were carried out. To establish the empirical relationship between SAR-derived parameters and collocated SWH, the sensitivity analysis of typical parameters about the normalized radar cross section (Nrcs) and imagery variance (Cvar) were performed to both VV and VH polarized images. Four scenes from GF-3 SAR imagery under typhoon conditions were used for training the model by the multivariate least square regression, and one scene was used for preliminary validation. It was found that the joint retrieval model based on VV and VH polarized SAR imagery performed better than any single polarized model. These results, verified by using ECMWF data, revealed the soundness of this approach, with a correlation of 0.95, bias of 0 m, RMSE of 0.44 and SI of 0.01 when VV polarization and VH polarization data were both used.

Key words Gaofen-3; SAR; typhoon; significant wave height

1 Introduction

In past decades, typhoons have been regarded as one of the most dangerous and destructive extreme meteorological phenomena, generally combined with bad disaster. Effective monitoring and capture to typhoon is important for safety of shipping and offshore oceanographic engineering. The research of typhoon can also reveal the mechanism of sea-air interaction and contribute to global climate issues. In terms of the extreme sea state caused by typhoons, the parameter of significant wave height (SWH) has been noticed and used in the research of typhoon. Therefore, it is important to develop the method of deriving SWH from remote sensing images. Of the remote sensing sensors, the synthetic aperture radar (SAR) technology has been shown to be valid to detect ocean surface significant wave height (SWH) because it is not affected by clouds and rain and has high spatial resolution (Chapron *et al*., 2011; Zhang *et al*., 2014; Zhang *et al*., 2015). Therefore, how to retrieve SWH from SAR imagery has been widely studied by researchers worldwide.

In early days, the non-linear imaging theory describing the relationship between SAR imagery and time-varying sea surface height was applied to derive the corresponding wave slope spectrum. To propose a non-linear modulation relationship, the modulation transfer functions (MTF), or namely titled, hydrodynamics and velocity bunching functions, have been explored for wave spectrum retrieval (Hasselmann and Hasselmann, 1991; Qiu *et al*., 2017).

Although the mathematical analysis methods have already been well applied to derive wave spectrum from SAR imagery, it is still difficult to acquire the first-guess wave spectrum (Hasselmann and Hasselmann, 1991; Sun and Guan, 2006). Due to the absence of precise first-guess spectrum, the analytical methods for SWH retrieval are limited. At present, the Max Planck Institute (MPI), the semi-parametric retrieval algorithm (SPRA), the partition rescaling and shift algorithm (PARSA), and the parameterized first-guess spectrum method (PFSM) have been applied for wave slope spectrum and SWH retrieval from SAR imagery (Engen and Johnsen, 1995; Mastenbroek and de Valk, 2000; He *et al*., 2004). For now, the retrieving results of SWH from the estimated wave spectrum of SAR imagery are not satisfying.

To satisfy the requirement of SWH retrieval precision, many researches focused on the empirical methods to directly establish the relationship between SAR imagery pa-

* Corresponding author. E-mail: han_bing@mail.ie.ac.cn

rameters and collocated SWH. It is proven that there is a quasi-linear relationship between normalized radar cross section (Nrcs) and SWH. To date, some studies have constructed empirical algorithms and acquired ocean SWH information from SAR imagery without any additional input (He *et al*., 2012; Shao *et al*., 2016). Initially, the empirical SWH retrieval method, namely CWAVE_ERS, was developed by using ERS-2 SAR imagery, which has a good performance in conditions of low and medium sea states (Schulz-Stellenfleth *et al*., 2005). Afterwards, with extending 22 types of imagery parameters, a new SWH retrieval method was proposed from Envisat ASAR and Sentinel-1 SAR imagery, denoted as CWAVE_ENV and CWAVE_S1A, respectively (Li *et al*., 2011; Stopa and Mouche, 2016). Besides the Nrcs, the cutoff wavelength was also found to have high correlation with SWH and can be well applied for SWH retrieval (Shao *et al*., 2017). Although empirical methods cannot explain the relationship between sea surface scattering and sea states, it is still significant to be adopted due to its high retrieval precision for SWH. As some new satellites were launched in recent years, more SWH retrieval methods are proposed based on different SAR data. Gaofen-3 (GF-3) satellite, launched in August 2016, was designed for marine monitoring and detection. Almost 12 types of imaging modes can be performed to sea surface observation. As a major application field for marine dynamics detection, the SWH retrieval has been the focus of many studies. A new empirical method for SWH retrieval was developed by using GF-3 SAR imagery, known as CSAR_WAVE (Zhu *et al*., 2018). Besides Nrcs and imagery variance (Cvar), the cutoff wavelength is also selected for model training and verifying. The known QPCWAVE_ GF3 method was trained based on HH, HV, VH, VV four polarization SAR imagery acquired by GF-3 SAR (Wang *et al*., 2018).

For now, GF-3 SAR is also widely used for marine typhoon monitoring. Data from several typhoons have been captured and recorded on many occasions, for example, Noru, Doksuri, Talim, and Hato *etc*. The research on typhoon SWH retrieval from GF-3 SAR by empirical methods is still in process (Shao *et al*., 2019; Shi *et al*., 2019). Due to the extreme sea states, traditional empirical method will not be well applied for SWH retrieval. The wave breaking term will be remarkable in wave physical equations. So, it is necessary to re-adjust the empirical relationship between SAR parameters and SWH data to improve the retrieval precision of SWH.

In this paper, a new empirical method to retrieve SWH under typhoon conditions was proposed based on GF-3 SAR-derived parameters. The matched dataset is presented in Section 2. A brief illustration of GF-3 SAR typhoon imagery and SWH parameters from the European Center for Medium-Range Weather Forecasts (ECMWF) reanalysis data was also presented. Before model training, the GF-3 SAR imagery under typhoon conditions is recalibrated and made de-scalloping to improve its quality in Section 3. In Section 4, with high-precision data of Nrcs from reprocessed imagery, an empirical relationship between derived-SAR parameters and ECMWF SWH is established and validated. The discussion and conclusions are given in Sections 5 and 6, respectively.

2 Materials and Methodology

2.1 Remote Sensing Data

The matched dataset consisted of five scenes of GF-3 SAR typhoon imagery in NSC and WSC modes. The details of the collected GF-3 dual polarization SAR imagery are shown in Table 1.

Table1 Details of GF-3 SAR imagery used in this paper

ID	Mode	Resolution (m)	Swath (m)	Polarization	Time (UTC)	Location	
						Longitude (˚W)	Latitude (˚N)
3389046	NSC	50	300	VV/VH	2017-03-02 16:41	161.18	26.12
3959036	WSC	100	500	VV/VH	2017-08-04 21:26	127.72	28.35
4019942	WSC	100	500	VV/VH	2017-08-22 22:23	113.07	20.64
4098505	WSC	100	500	VV/VH	2017-09-16 09:34	127.95	27.62
5356932	WSC	100	500	VV/VH	2018-08-01 09:34	128.67	27.78

The location of typhoons captured by GF-3 SAR are shown in Fig.1. Three out of five SAR images were captured in the East China Sea, one was obtained in the South China Sea, and another was gotten in the Pacific Ocean. The typhoons, named TALIM, NORU, HATO, DOKSURI, JONGDARI, were effectively captured in the collected SAR imagery. Unfortunately, there were no *in-situ* buoys matching the SAR footprints. Therefore, ERA-Interim reanalysis data was chosen as reference data, which provides SWH at a $0.125^{\circ} \times 0.125^{\circ}$ grid resolution every six hours. Most studies have validated the precision of ERA-Interim data under different sea states (Wan *et al*., 2015). SWH data from ECMWF can therefore be regarded as true SWH values.

2.2 Methodology

An empirical method is proposed to derive SWH from matched SAR imagery. Main steps were given in the flowchart of Fig.2.

3 Preprocessing of the GF-3 SAR Imagery

In this section, the GF-3 SAR imagery was recalibrated and made de-scalloping to improve the image quality and acquire precise Nrcs images under typhoon conditions.

3.1 Recalibration over Rainforest

The GF-3 SAR calibration was based on the engaged

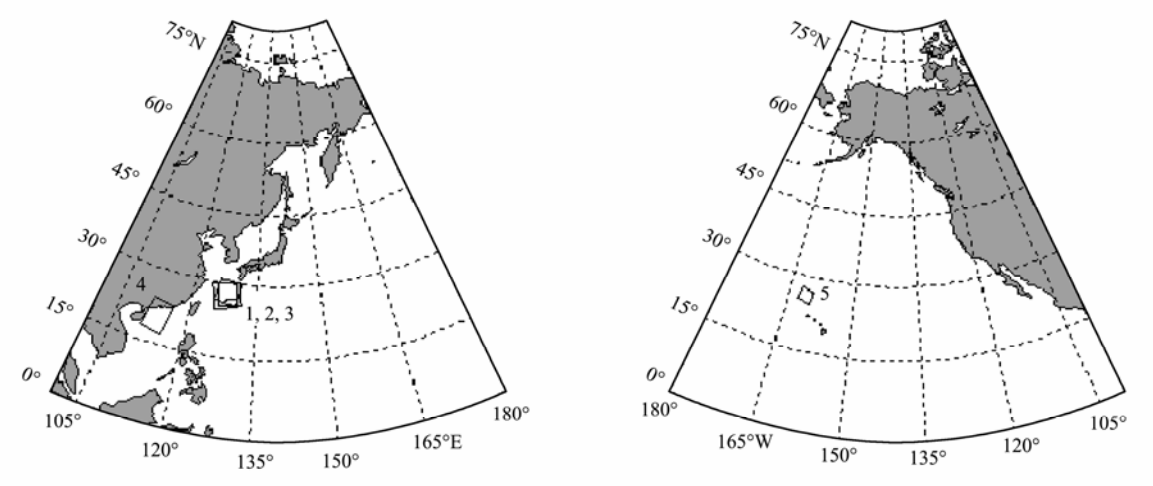

Fig.1 The locations of the collected SAR imagery. ID 1 corresponds to typhoon TALIM; ID 2 corresponds to typhoon NORU; ID 3 corresponds to typhoon HATO; ID 4 corresponds to typhoon DOKSURI; ID 5 corresponds to typhoon JONGDARI.

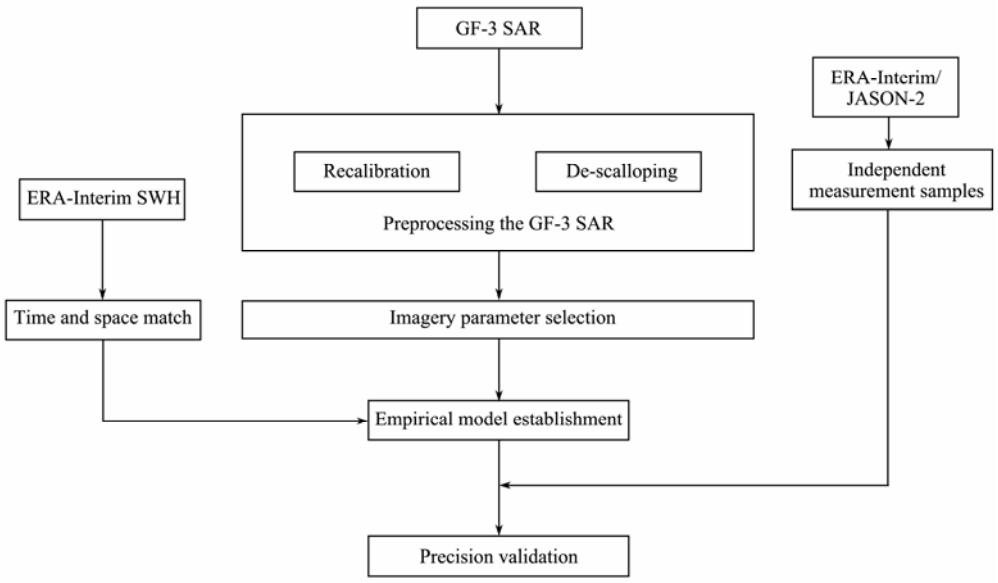

Fig.2 Flowchart of the SWH retrieval method proposed in this paper.

calibration algorithm, listed as follows (Shang *et al*., 2018):

$$\sigma_{dB}^{0} = 10\log_{10}(P^{I} \times (\text{QualifyValue}/32767)^{2}) - K_{dB}\,, \quad (1)$$

where $P^{I} = I^{2} + Q^{2}$, and I represents the real part of SLC image, Q represents the imagery part of SLC image, QualifyValue represents the maximum of quantified imagery, and K_{dB} represents the calibration constant. Considering that the sea surface is highly dynamic, distributed and has a low scattering scene, the traditional corner reflector and active calibration equipment are not well applied to acquire sea surface Nrcs from GF-3 SAR imagery. It is necessary to adopt another method to recalibrate Nrcs from SAR imagery. For C-band SAR, the Amazon rain forest is usually used as natural object to examine the precision of Nrcs due to the stability of structure and state (Li *et al*., 2019; Wang *et al*., 2019). Here the VV and VH polarized GF-3 SAR images over the Amazon rain forest are shown in Fig.2.

Considering the beam design of NSC and WCS modes, the influence of incidence angle θ can be expressed as follows (Li *et al*., 2019):

$$\sigma^{0} = \gamma^{0}\cos(\theta) = \beta^{0}\tan(\theta)\,, \quad (2)$$

where γ^{0}, σ^{0}, and β^{0} represent the different forms of Nrcs characteristics. In terms of isotropic properties of rainforests, γ^{0} can be approximately incidence angle-independent. To recalibrate the GF-3 SAR imagery, the VV and VH polarization calibration constants were acquired by fitting the image intensity of rainforest to the γ^{0} value of Amazon rain forest. In Figs.3(a) and (b), 512×512 sub-images were calculated by using a moving window. In this paper, the VV and VH polarization sub-image intensity along the range direction are shown in Fig.4. The new calibration constants were applied and recalibration was performed on the collected GF-3 SAR imagery in this paper.

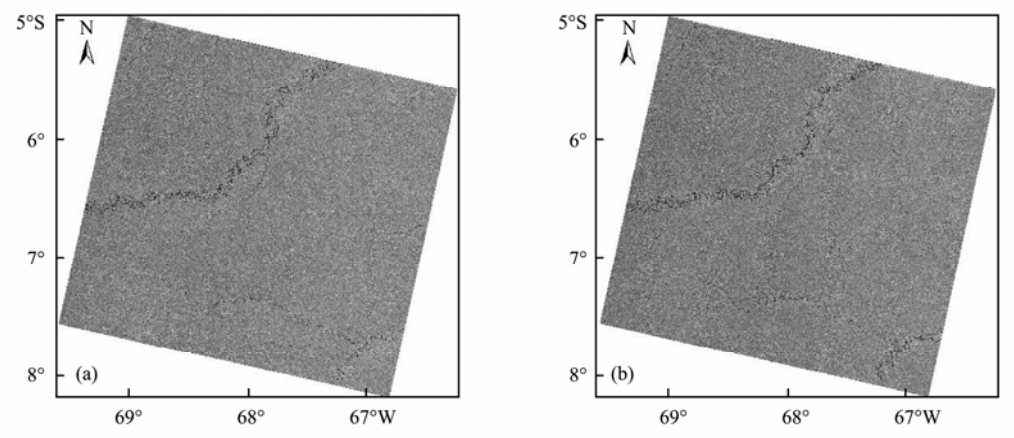

Fig.3 The GF-3 SAR images over the Amazon rain forest. (a) represents the VV polarization, and (b) represents the VH polarization. The images were acquired in 2017-02-25 10:16 (UTC).

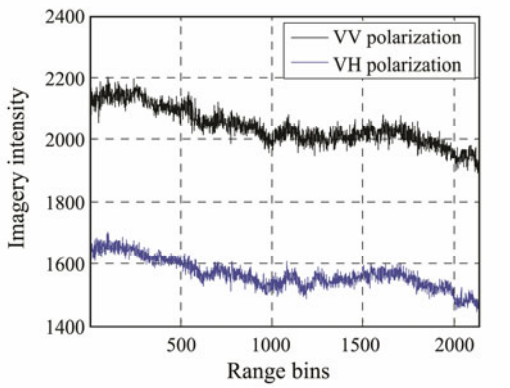

Fig.4 The rainforest imagery intensity of GF-3 SAR for both VV and VH polarizations.

3.2 De-Scalloping

Another important issue in preprocessing of GF-3 SAR images is de-scalloping. Because of periodic switching between sub-swatches, a wavelike periodic modulation occurs along the azimuth direction. The scalloping disturbs the sea surface wave strip, even affecting the image quality. To acquire precise sea surface Nrcs, a new de-scalloping method was applied to suppress the scalloping (Romeiser *et al*., 2013; Zhong *et al*., 2020). The period modulation of scalloping can be expressed as:

$$I(x)=\sigma(x)\sum_{i=1}^{N}Sca(x-i\times N_p)\,. \tag{3}$$

In log domain, the imagery $I(x)$ can be re-arranged as:

$$I_{\log}(x)=10\times\log_{10}\sigma(x)+10\times\log_{10}\sum_{i=1}^{N}Sca(x-i\times N_p)\,. \tag{4}$$

By the transformation of imagery $I_{\log}(x)$ from imagery domain to frequency domain, then the azimuth spectrum can be separated to a real spectrum $F_\sigma(k)$ and a residual scalloping spectrum $F_{Sca}(k)$.

$$F(k)=F_\sigma(k)+F_{Sca}(k)\,. \tag{5}$$

Due to the periodic character of scalloping, the azimuth spectrum can be re-expressed by using a set of equal-spaced harmonics as the following equation:

$$k_i=\frac{i\times N_{FFT}}{N_p}(-N_p/2\le i\le N_p/2)\,, \tag{6}$$

where k_i denotes the position of i-th harmonic in the frequency domain, and N_{FFT} denotes the number of points involved in the Fast Fourier Transform (FFT).

The original and de-scalloped GF-3 SAR images are shown in Fig.5. Before de-scalloping, the sea surface images were deteriorated by the wavelike scallop, which was parallel to the range direction. The real wave direction was obscured in both VV and VH polarizations. As seen in Fig.4, the wave direction and wave strips were clearly identified after scallop removal.

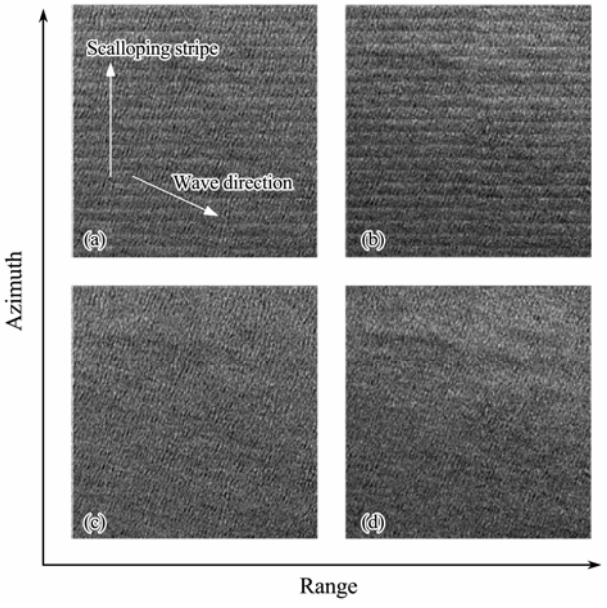

Fig.5 GF-3 SAR sea surface images before and after de-scalloping. (a), VV polarization before de-scalloping; (b), VH polarization before de-scalloping; (c), VV polarization after de-scalloping; (d), VH polarization after de-scalloping.

In terms of empirical SWH retrieval, the wave direction from SAR imagery was not involved in the established model. Moreover, the influence of scallops on Nrcs needed to be preliminarily assessed. As seen in Fig.6, Nrcs data before and after de-scalloping along the range direction were compared. The error declined by 0.44 dB after de-scalloping along the azimuth direction.

By making recalibration and de-scalloping to the raw GF-3 SLC imagery, the image quality was improved and typhoon scenes can be clearly identified in final imagery. Five typhoon scenes were re-imaged for both VV and VH polarizations, as shown in Fig.7. It can be seen that image quality under typhoon conditions improved significantly. Although some areas in the SAR imagery of Fig.7e were still affected by radar echo, the preprocessing to the raw GF-3 SAR images was still beneficial to the SWH retrieval.

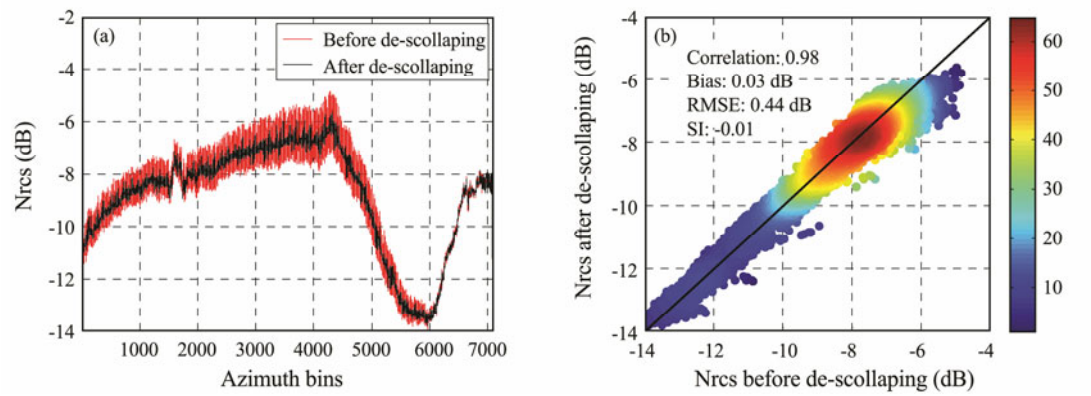

Fig.6 Nrcs curves before and after de-scalloping. (a), Nrcs variation as the function of azimuth bins; (b), comparison of Nrcs before and after de-scalloping.

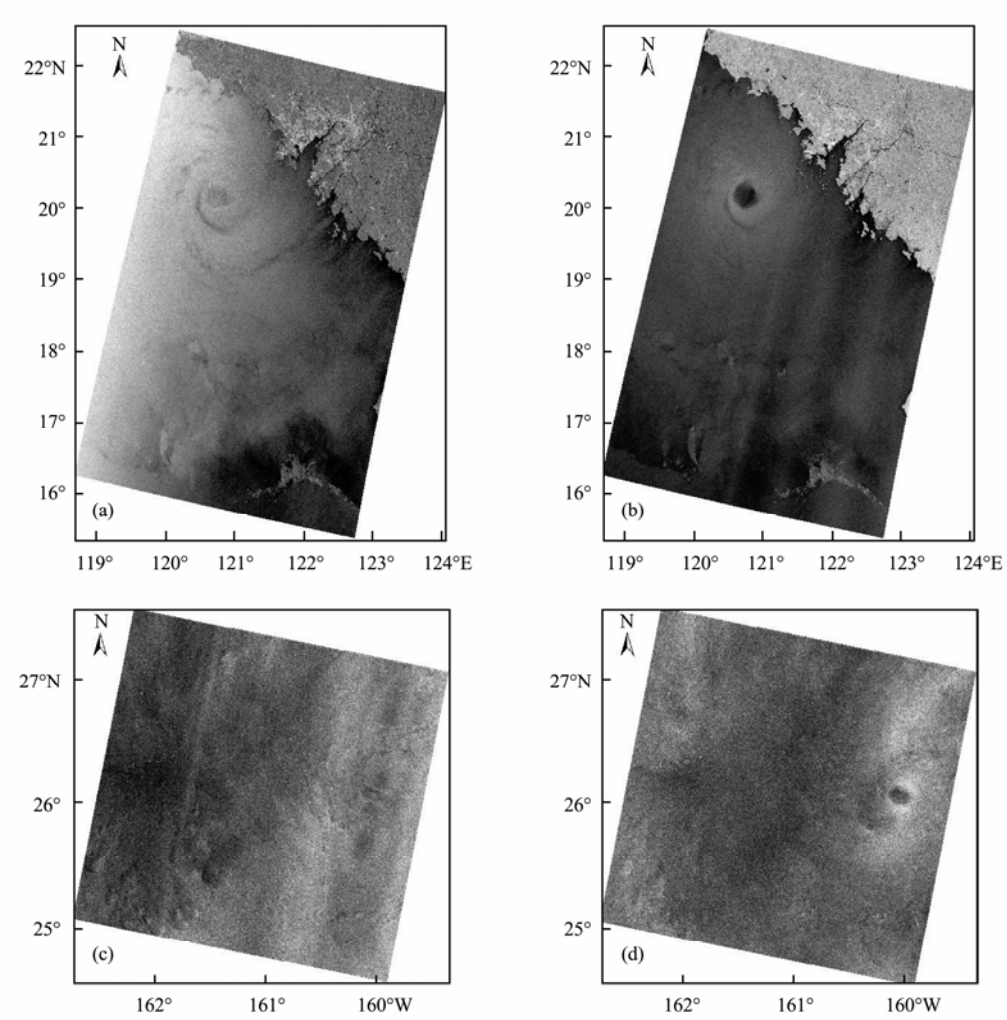

Fig.7 (a)–(d) Re-processed GF-3 SAR typhoon imagery for both VV (left column) and VH polarizations. (a) and (b), the GF-3 SAR NSC mode imagery of typhoon Lionrock acquired on 2017-5-2 at 16:41; (c) and (d), the GF-3 SAR WSC mode imagery from typhoon NORU on 2017-8-4 at 21:26.

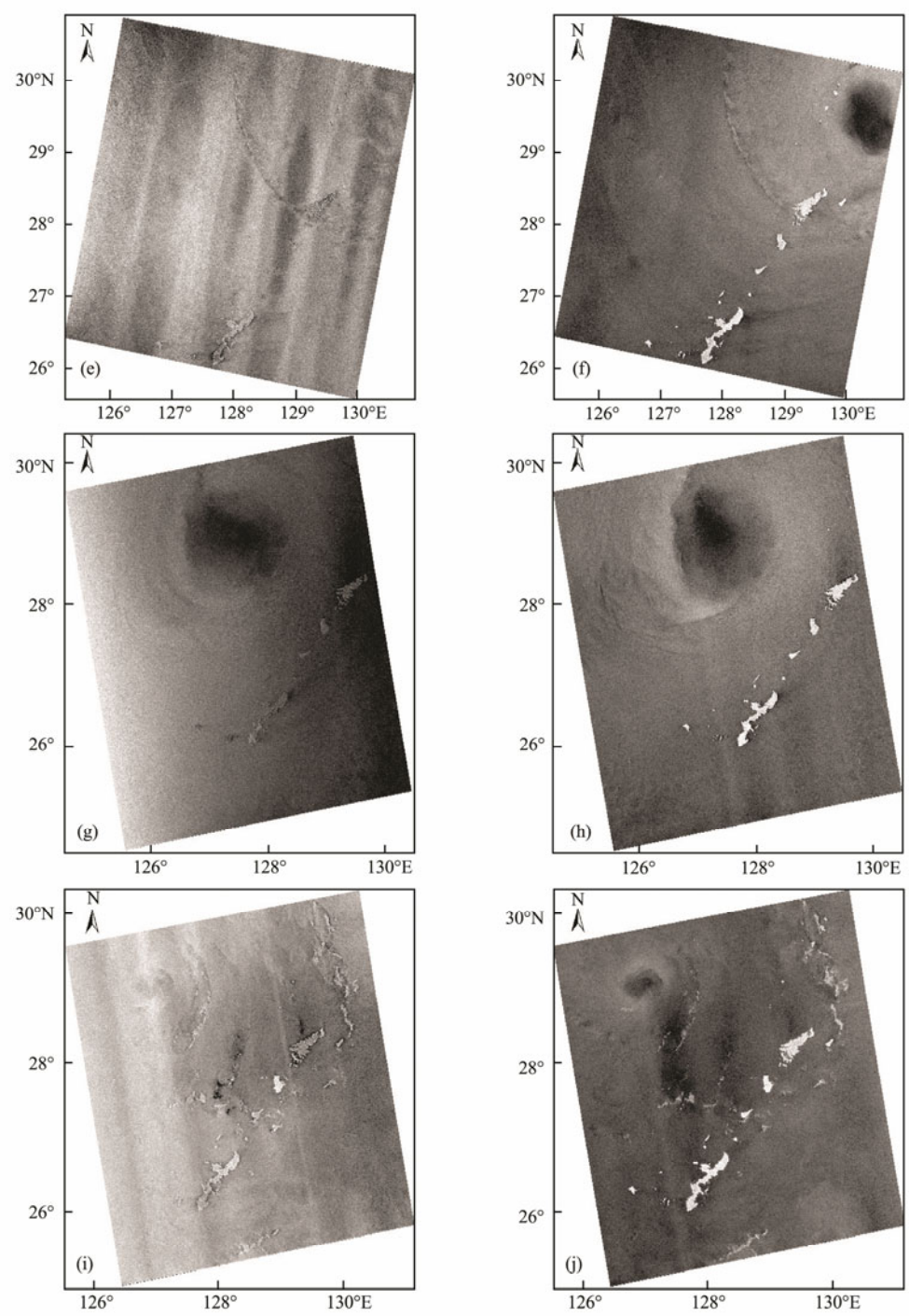

Fig.7 (e)−(j) Re-processed GF-3 SAR typhoon imagery for both VV (left column) and VH polarizations. (e) and (f), the GF-3 SAR WSC mode imagery from typhoon HATO acquired on 2017-8-22 at 22:23; (g) and (h), the GF-3 SAR WSC mode imagery of typhoon DOKSURI acquired on 2017-9-16 at 09:34; (i) and (j), the GF-3 SAR WSC mode imagery of typhoon JONGDARI acquired on 2018-8-1 at 09:34.

4 Retrieval of SWH from GF-3 SAR

In this section, a new empirical typhoon SWH retrieval method from GF-3 SAR is proposed and validated with reanalysis SWH data provided by ERA-Interim.

4.1 Imagery Parameter Selection

Following the CWAVE_S1 approach from Schulz-Stellenfleth, we separated the SAR imagery spectrum into series of orthogonal harmonic components by using Gegenbauer polynomials fitting. A total of 22 parameters were derived from the CWAVE_S1 approach, which consisted of two types of parameters in the imagery domain and 20 types of parameters in the frequency domain. These can be expressed as (Li *et al*., 2011; Gao *et al*., 2018):

$$\sigma^0 = 10\log_{10}(\langle I\rangle)\,, \tag{7}$$

$$\mathrm{Cvar}=\left(std2\left(\frac{I-\langle I\rangle}{\langle I\rangle}\right)\right)^2, \tag{8}$$

$$S_i=\int_A \bar{P}(k_x,k_y)\bar{h}_i(k_x,k_y)\mathrm{d}k_x\mathrm{d}k_y,\ 1\le i\le 20, \tag{9}$$

where I represents the calibrated SAR imagery intensity, $\langle\rangle$ represents the mathematical operation of average, $\bar{P}$ represents the normalized SAR imagery spectrum, $\bar{h}$ represents the orthogonal function by using Gegenbauer polynomials fitting, and (k_x, k_y) are the wavenumbers for the range and the azimuth direction, respectively. The orthogonal function $\bar{h}$ can be decomposed into a set of harmonic functions as follows (He *et al*., 2015):

$$h_{ij}(\alpha_k,\alpha_\varphi)=\eta(k_x,k_y)g_i(\alpha_k)f_j(\alpha_\varphi),\quad 1\le i\le 4,\ 1\le j\le 5, \tag{10}$$

$$g_{n_k}=\sqrt{\frac{n_k+3/2}{(n_k+2)(n_k+1)}}C_{n_k}^{3/2}\sqrt{1-\alpha_k^2}, \tag{11}$$

$$f_{n_\varphi-1}(\alpha_\varphi)=\sqrt{\frac{2}{\pi}}\sin((\alpha_\varphi-1)\alpha_\varphi), \tag{12}$$

$$f_{n_\varphi}(\alpha_\varphi)=\sqrt{\frac{2}{\pi}}\cos((\alpha_\varphi-1)\alpha_\varphi), \tag{13}$$

where $g_i(\alpha_k)$ and $f_j(\alpha_\varphi)$ represent the Gegenbauer polynomials and harmonic functions, respectively, $\eta(k_x, k_y)$ denotes the weight variables, $g_i(\alpha_k)$ denotes the general expression of Gegenberg polynomials, n_k=1, 2, 3, 4 and in this paper. However, the method in the frequency domain did not have satisfying performance for SWH retrieval in the previous study (Shao *et al*., 2019). Therefore, in this study, only Nrcs and Cvar were used to establish the empirical relationship with SWH. Because the dual-polarization channel was provided by GF-3 SAR, the VV and VH polarized images were used to explore the correlation between Nrcs of GF-3 and the matched SWH parameter.

Fig.8 shows the response of Nrcs to SWH from VV and VH polarizations, respectively. An approximately linear

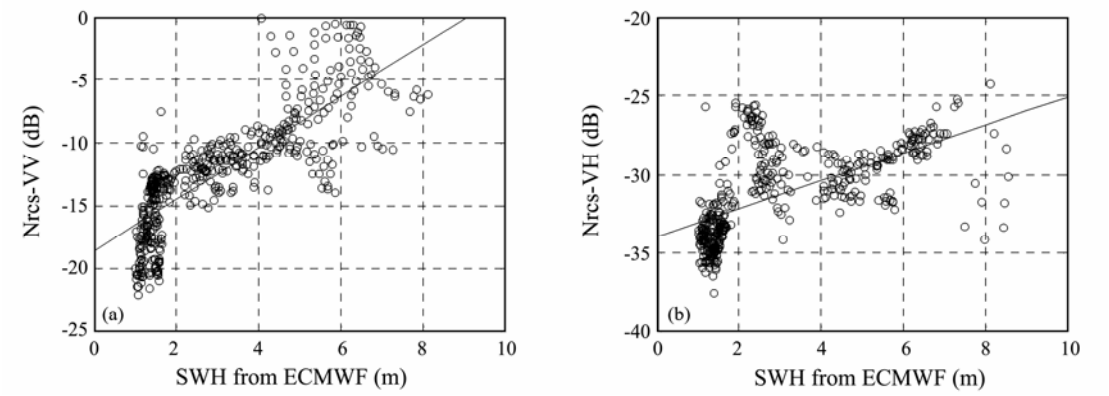

Fig.8 The response of Nrcs to SWH for both VV and VH polarizations. (a), VV polarization; (b), VH polarization.

was presented in Figs.8(a) and (b). In addition to the significant response of Nrcs of VV polarization to SWH, it is interesting to found that the VH polarization also had similar performance with increasing SWH.

4.2 Establishment of a New Empirical Model

A new empirical relationship is suggested to retrieve the SWH by using GF-3 SAR-derived parameters as inputs. To improve modeling precision, the multivariate least squares algorithm is performed for model fitting (Wang *et al*., 2014). It is noticed that Nrcs and Cvar of VV and VH polarization were selected for model establishment with Eq. (14).

$$SWH=A_0+\sum_{i=1}^{n}A_i\times S_i+\sum_{i,j=1}^{n}A_{i,j}\times S_i\times S_j. \tag{14}$$

Four out of five GF-3 SAR typhoon scenes were used to train the empirical relationship. Before model training, it was important to perform a check for homogeneity to exclude the influence of non-wave phenomena, such as oil spills, upwelling, atmospheric gravity wave, *etc*. (Cao *et al*., 2019). Especially in an extreme sea state, the Nrcs variability will decrease the model training precision. To acquire effective training samples, a new parameter, called Spectral Peak Saliency (SPS), was used to check for the homogeneity of GF-3 SAR typhoon imagery (Ding *et al*., 2019). The SPS is defined as the ratio of spectral peak to background average in the frequency domain. By SPS criteria, the train samples were collocated with ERA-Interim SWH and fitted by using a multivariate least square regression function.

4.3 Validation

According to the established empirical model, a GF-3 SAR typhoon scene was used to verify the retrieval precision. The dual polarized GF-3 SAR imagery for typhoon DOKSURI was used to assess model precision. The corresponding SWH distribution is shown in Fig.9.

The retrieval SWH results from VV and VH polarizations are shown in Fig.10. For VV polarization, a strong correlation of 0.88 with a bias of 0 m was obtained between

GF-3 SAR-derived SWH and ECMWF provided SWH. Interestingly, the estimated SWH from VH polarization revealed the capability of SAR cross-channel for SWH retrieval. Although the retrieval results from the VH polarized GF-3 SAR imagery were not as good as those from the VV polarization, they were still meaningful and VH polarization has the potential to be used to retrieve SWH from GF-3 (Fan *et al*., 2019).

Taken into Eq. (10), the VV and VH polarizations of GF-3 SAR imagery were co-used for model establishment and verification. The verification is based on the GF-3 SAR imagery of typhoon DOKSURI in Fig.9. The retrieval results are shown in Fig.10. It can be seen that the retrieval precision was improved, with a correlation of 0.95, a bias of 0 m, RMSE of 0.44 m and SI of 0.01.

5 Selection of Training Samples

5.1 Selection of Training Samples

Because the relationships between Nrcs and SWH were established by empirical fitting, it is important to discuss the influence of sample selection on model precision. According to selection criteria used in this paper, the SPS can be expressed as:

$$SPS = \frac{\mathrm{var}(\hat{\Phi}(k))}{(\mathrm{mean}(\hat{\Phi}(k)))^2}. \quad (15)$$

According to the empirical relationship, the threshold value of SPS was set to 1.6 in this paper. Actually, the established model precision mostly depended on the quality of verification samples. The model precision with different SPS thresholds is shown in Table 2.

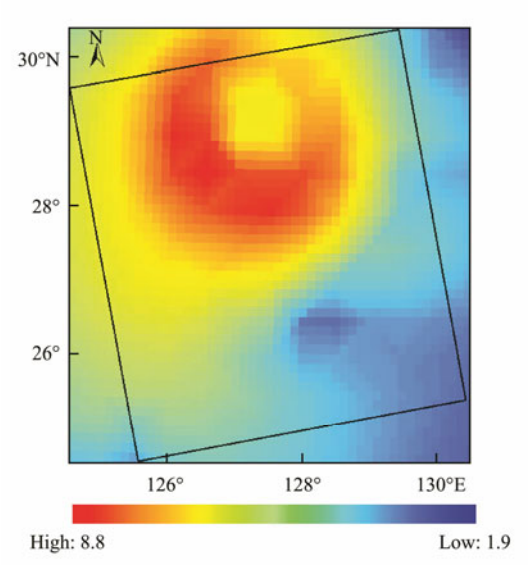

Fig.9 The SWH distribution of typhoon DOKSURI. Colors represent SWH values.

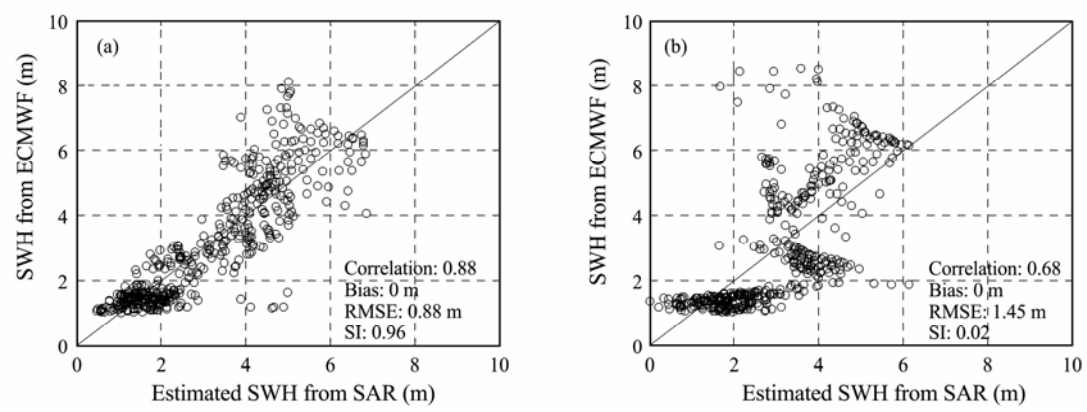

Fig.10 Retrieval results for VV and VH polarizations. (a), VV polarization; (b), VH polarization.

Table 2 Model precision with different SPS thresholds used in this paper

SPS threshold	Model samples	Model precision		
		Correlation	Bias (dB)	RMSE (dB)
2.2	834	0.74	0.01	1.38
2.0	685	0.78	0.01	1.27
1.8	481	0.88	0.01	0.88
1.6	230	0.88	0.01	0.88
1.4	90	0.93	0.01	0.41
1.2	18	0.97	0.01	0.34

It is noted that as threshold increased, the number of training samples increased and the precision of training results gradually decreased. It can be attributed to the fact that more sub-images that did not pass the homogenous check were used for empirical model training. Therefore, the number and quality of the training samples are important in model training. In fact, in our previous study, the threshold value was set to 1.05 according to ENVISAT ASAR data (Gao *et al*., 2018). It appears that how to set a SPS threshold was related to the precision of SAR imagery quantification. It seems that a self-adaption method for the SPS selection should be developed and further discussed.

6 Conclusions

The retrieval methods of wave parameters, especially SWH from SAR, have been the focused topic in recent years. Although many methods have been proposed to improve the retrieval precision, it is still difficult to ac-

quire SWH information from SAR imagery, especially in extreme sea states. In addition, the influence of SAR radiometric quality on SWH retrieval cannot be neglected yet. Along with the launch of GF-3 SAR, several typhoon scenes were acquired in WSC mode, which provides the best possible for SWH retrieval in high sea states.

In this paper, the capability of GF-3 SAR for SWH retrieval under typhoon conditions is verified. To explore the SWH retrieval method, the GF-3 SAR images under typhoon conditions are collected to match the ECMWF reanalysis SWH data. First, considering the GF-3 imagery quality, we recalibrate the GF-3 imagery by rainforest and remove the influence of scalloping. Second, the correlation of Nrcs based on the VV and VH polarization with collocated SWH was assessed to investigate the possibility of these two kinds of polarized images for SWH retrieval. Then, four scenes of GF-3 SAR imagery were used to train the model by using a multivariate least square regression for VV and VH polarizations. A joint retrieval model was also proposed for VV and VH polarized SAR imagery, which performed better than single polarization. Finally, another typhoon scene of GF-3 SAR imagery and collocated ECMWF data were used to verify the retrieval scheme. Retrieval results demonstrated the soundness of the SWH retrieval process, which have a correlation of 0.95 with ECMWF data and a bias of 0 m, a RMSE of 0.44 and SI of 0.01 when VV and VH polarization data were co-used. In conclusion, the empirical method used in this paper is effective to derive SWH from GF-3 SAR imagery under typhoon conditions, although the good result still relies on the good-quality of sub-images in model. In future studies, the effectiveness of VH polarization imagery needs to be explained and more images under the typhoon conditions are worth to be acquired to improve the method soundness. Moreover, the influence of wave breaking also will be involved to SAR wind and wave retrieval in further.

Acknowledgements

This work was funded by the National Natural Science Foundation of China (No. 4197060692). ECMWF wave fields were accessed *via* http://www.ECMWF.int. The information on cyclones provided by NOAA was downloaded *via* https://coast.noaa.gov/hurricanes.

References

Cao, C., Sun, J., and Zhang, W., 2019. The correlation analysis between images stripe definition and inversion parameters error in ASAR wave mode. *Oceanology et Limnology Sinica*, **50** (4): 777-787 (in Chinese with English abstract).

Chapron, B., Johnsen, H., and Garello, R., 2011. Wave and wind retrieval from SAR images of the ocean. *Annales Des Télécommunications*, **56** (11): 682-699.

Ding, Y., Zuo, J., Shao, W., Shi, J., Yuan, X. Z., Sun, J., *et al*., 2019. Wave parameters retrieval for dual-polarization C-band synthetic aperture radar using a theoretical-based algorithm under cyclonic conditions. *Acta Oceanologica Sinica*, **38** (5): 21-31.

Engen, G., and Johnsen, H., 1995. SAR-ocean wave inversion using image cross spectra. *IEEE Transactions on Geoscience and Remote Sensing*, **33** (4): 1047-1056.

Fan, C., Wang, X., and Zhang, X., 2019. A newly developed ocean significant wave height retrieval method from Envisat ASAR wave mode imagery. *Acta Oceanologica Sinica*, **38** (9): 120-127.

Gao, D., Liu, Y., Meng, J., Jia, Y. G., and Fan, C., 2018. Estimating significant wave height from SAR imagery based on an SVM regression model. *Acta Oceanologica Sinica*, **37** (3): 103-110.

Hasselmann, K., and Hasselmann, S., 1991. On the nonlinear mapping of an ocean wave spectrum into a synthetic aperture radar image spectrum and its inversion. *Journal of Geophysical Research: Oceans*, **96** (C6): 10713-10729.

He, L., Fablet, R., Chapron, B., and Touradre, J., 2015. Learning-based emulation of sea surface wind fields from numerical model outputs and SAR data. *IEEE Journal of Selected Topics in Applied Earth Observations and Remote Sensing*, **8** (10): 4742-4750.

He, W., Zhu, J., Yang, J., and Shi, C., 2012. A semiempirical algorithm for SAR wave height retrieval and its validation using Envisat ASAR wave mode data. *Acta Oceanologica Sinica*, **31**: 59-66.

He, Y., Perrie, W., Tao, X., and Zou, Q., 2004. Ocean wave spectra from a linear polarimetric SAR. *IEEE Transactions on Geoscience and Remote Sensing*, **42** (11): 2623-2631.

Li, H., Mouche, A., Stopa, J. E., and Chapron, B., 2019. Calibration of the normalized radar cross section for Sentinel-1 wave mode. *IEEE Transactions on Geoscience and Remote Sensing*, **57** (3): 1514-1522.

Li, X. M., Lehner, S., and Bruns, T., 2011. Ocean wave integral parameter measurements using Envisat ASAR wave mode data. *IEEE Transactions on Geoscience and Remote Sensing*, **49** (1): 155-174.

Mastenbroek, C., and de Valk, C. F., 2000. A semiparametric algorithm to retrieve ocean wave spectra from synthetic aperture radar. *Journal of Geophysical Research*, **105** (C2): 3497-3516.

Qiu, J., Zhang, B., Chen, Z., and He, Y., 2017. A new modulation transfer function with range and azimuth dependence for ocean wave spectra retrieval from X-band marine radar observations. *IEEE Geoscience and Remote Sensing Letters*, **14** (8): 1373-1377.

Romeiser, R., Horstmann, J., Caruso, M. J., and Graber, H. C., 2013. A descalloping postprocessor for scanSAR images of ocean scenes. *IEEE Transactions on Geoscience and Remote Sensing*, **51** (6): 3259-3272.

Schulz-Stellenfleth, J., Lehner, S., and Hoja, D., 2005. A parametric scheme for the retrieval of two-dimensional ocean wave spectra from synthetic aperture radar look cross spectra. *Journal of Geophysical Research: Oceans*, **110** (C5): C05004.

Shang, M., Han, B., Ding, C., Sun, J., Zhang, T., Huang, L., *et al*., 2018. A high-resolution SAR focusing experiment based on GF-3 staring data. *Sensors*, **18** (4): 943.

Shao, W., Ding, Y., Li, J., Gou, S. P., Nunziata, F., Yuan, X. Z., *et al*., 2019. Wave retrieval under typhoon conditions using a machine learning method applied to Gaofen-3 SAR imagery. *Canadian Journal of Remote Sensing*, **45** (6): 723-732.

Shao, W., Sheng, Y., and Sun, J., 2017. Preliminary assessment of wind and wave retrieval from Chinese Gaofen-3 SAR imagery. *Sensors*, **17** (8): 1705.

Shao, W., Zheng, Z., Li, X., and Li, H., 2016. Ocean wave parameters retrieval from Sentinel-1 SAR imagery. *Remote Sensing*, **8** (9): 707-721.

Shao, W., Zhu, S., Sun, J., Yuan, X. Z., Sheng, Y., Zhang, Q. J., *et al*., 2019. Evaluation of wind retrieval from co-polarization Gaofen-3 SAR imagery around China seas. *Journal of Ocean University of China*, **18**: 80-92.

Shi, J., Hu, J., Shao, W., Wang, X. Q., Yuan, X. Z., Zhao, L. B., *et al*., 2019. The impact of rain to observed signal from Chinese Gaofen-3 synthetic aperture radar in typhoons. *Acta Oceanologica Sinica*, **38** (11): 121-133.

Stopa, J. E., and Mouche, S., 2016. Significant wave heights from Sentinel-1 SAR: Validation and applications. *Journal of Geophysical Research: Oceans*, **122** (3): 1827-1848.

Sun, J., and Guan, C., 2006. Parameterized first-guess spectrum method for retrieving directional spectrum of swell-dominated waves and huge waves from SAR images. *Chinese Journal of Oceanology and Limnology*, **24** (1): 14-22.

Wan, Y., Zhang, J., Meng, J., and Wang, J., 2015. Exploitable wave energy assessment based on ERA-interim reanalysis data – A case study in the East China Sea and the South China Sea. *Acta Oceanologica Sinica*, **34** (9): 143-155.

Wang, H., Li, H., Lin, M., Zhu, J. H., Wang, J., Li, W. W., *et al*., 2019. Calibration of the copolarized backscattering measurements from Gaofen-3 synthetic aperture radar wave mode imagery. *IEEE Journal of Selected Topics in Applied Earth Observations and Remote Sensing*, **12** (6): 1748-1762.

Wang, H., Wang, J., Yang, J., Ren, L., Zhu, J., Yuan, X., *et al*., 2018. Empirical algorithm for significant wave height retrieval from wave mode data provided by the Chinese satellite Gaofen-3. *Remote Sensing*, **10** (3): 363-386.

Wang, X., Chong, J., Yu, X., and Liu, L., 2014. Estimation bias of ocean current measured by along-track interferometric synthetic aperture radar and its compensation methods. *International Journal of Remote Sensing*, **35** (11-12): 4064-4085.

Zhang, B., Perrie, W., Zhang, J. A., Uhlhorm, E. W., and He, Y., 2014. High-resolution hurricane vector winds from C-band dual-polarization SAR observations. *Journal of Atmospheric and Oceanic Technology*, **31** (2): 272-286.

Zhang, X., Dierking, W., and Zhang, J., 2015. A polarimetric decomposition method for ice in the Bohai Sea using C-band PolSAR data. *IEEE Journal of Selected Topics in Applied Earth Observations and Remote Sensin*g, **8** (1): 47-66.

Zhong, L. H., Qiu, X. L., Han, B., and Hu, Y. X., 2020. An improved descalloping method combined with imaging parameters for GaoFen-3 scanSAR. *Remote Sensing*, **12** (5): 822-845.

Zhu, S., Shao, W., Armando, M., Shi, J., Sun, J., Yuan, X. Z., *et al*., 2018. Evaluation of Chinese quad-polarization Gaofen-3 SAR wave mode data for significant wave height retrieval. *Canadian Journal of Remote Sensing*, **44** (6): 588-600.

(Edited by Chen Wenwen)